CHEMISTRY OF MATERIALS

pubs.acs.org/cm

Article

Covalent Organic Framework Nanosheets Embedding Single Cobalt Sites for Photocatalytic Reduction of Carbon Dioxide

Xiaoyan Wang, Zhiwei Fu, Lirong Zheng, Chengxi Zhao, Xue Wang, Samantha Y. Chong, Fiona McBride, Rasmita Raval, Matthew Bilton, Lunjie Liu, Xiaofeng Wu, Linjiang Chen,* Reiner Sebastian Sprick,* and Andrew I. Cooper*

Cite This: https://dx.doi.org/10.1021/acs.chemmater.0c01642

Read Online

ACCESS | Metrics & More | Article Recommendations | Supporting Information

ABSTRACT: Covalent organic framework nanosheets (CONs), fabricated from two-dimensional covalent organic frameworks (COFs), present a promising strategy for incorporating atomically distributed catalytic metal centers into well-defined pore structures with desirable chemical environments. Here, a series of CONs was synthesized by embedding single cobalt sites that were then evaluated for photocatalytic carbon dioxide reduction. A partially fluorinated, cobalt-loaded CON produced 10.1 μmol carbon monoxide with a selectivity of 76%, over 6 hours irradiation under visible light (TON = 28.1), and a high external quantum efficiency (EQE) of 6.6% under 420 nm irradiation in the presence of an iridium dye. The CONs appear to act as a semiconducting support, facilitating charge carrier transfer between the dye and the cobalt centers, and this results in a performance comparable with that of the state-of-the-art heterogeneous catalysts in the literature under similar conditions. The ultrathin CONs outperformed their bulk counterparts in all cases, suggesting a general strategy to enhance the photocatalytic activities of COF materials.

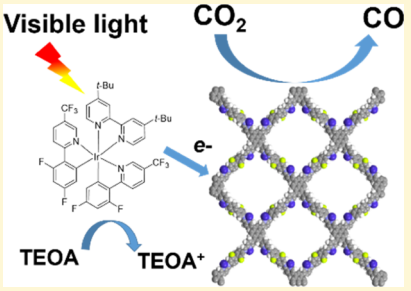

INTRODUCTION

The conversion of carbon dioxide into chemical fuels is thought to be one potential avenue to address the rising levels of CO_2 in the atmosphere and the rising energy demand of our growing population.[1−3] Photocatalytic reduction of CO_2 has been extensively studied using homogeneous[4,5] and heterogeneous catalysts.[6−8] Homogeneous catalysts usually possess high initial photocatalytic activity and selectivity for the desired products, but they are often not stable during extended operations. The use of expensive precious metals, coupled with the difficulty in catalyst recovery and product separation, makes such homogeneous catalysis reactions expensive.[9,10] Heterogeneous catalysts can address some of these issues because they can be isolated by simple filtration and can show good stability but are often hampered by their relatively low catalytic activity. One strategy to achieve the combined advantages of homo- and heterogeneous catalysis reactions is to anchor individual catalytic metal centers on supports, yielding the so-called single-atom or single-site catalysts. It is, however, a significant challenge to construct robust single-atom catalysts, which requires the mononuclear metal complexes or single metal atoms to be atomically distributed and strongly bound to the support, ideally also incorporating functional synergy between the catalytic sites and the support. Recently, metal−organic frameworks (MOFs)[11−13] and covalent organic frameworks (COFs)[14−16] have been reported incorporating single-atom catalysts. Their well-defined pore structures can be tuned to provide optimal confinement of known, catalytically active coordination metal complexes.[1,17,18]

Alternatively, molecular catalysts can be chemically tethered together in the form of a COF or MOF to afford heterogeneous catalysts, possessing spatially arranged catalytic sites and a precise control of the chemical environment around them.[14,19,20] MOFs have been shown to be active for photocatalytic CO_2 reduction, producing CO or formate.[21−24] Similarly, two-dimensional (2D) COFs have been reported as highly active photocatalysts for hydrogen production[25−27] and CO_2 reduction,[14,28,29] and they have the potential to be ideal supports for anchoring atomically distributed metal centers. Comparing COFs to MOFs, the former are composed of covalent bonds rather than coordination bonds, often making (though not always) them more stable. COFs can be conjugated in two dimensions, unlike MOFs which are usually not, offering a faster response to photoexcitation.[14] Moreover, COFs can be exfoliated, further increasing the surface area that can be in contact with the reaction medium. Also, COFs often have narrow band gaps, allowing efficient utilization of the solar spectrum.

Received: April 17, 2020
Revised: October 5, 2020

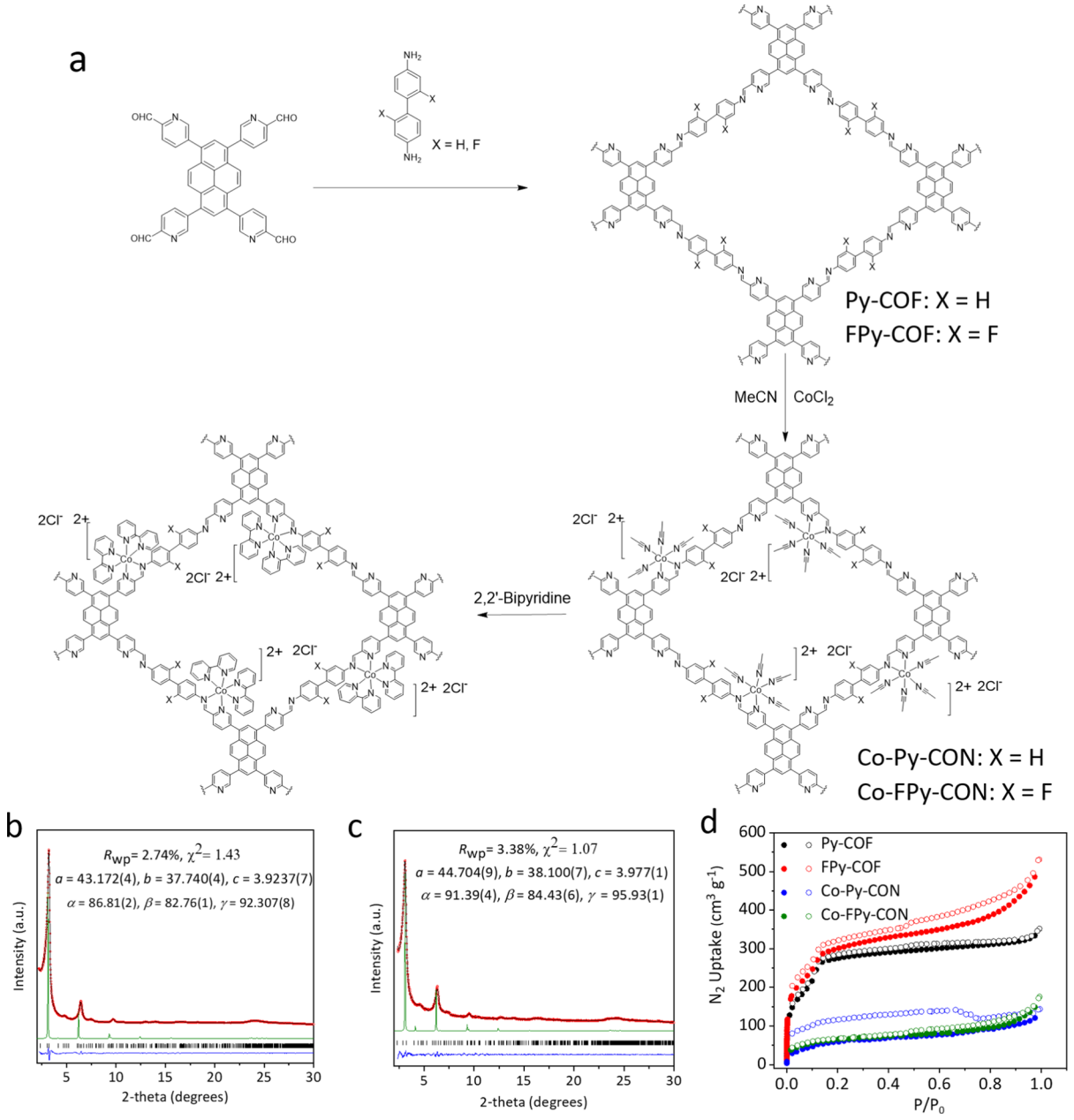

Figure 1. (a) Synthesis of Py-COF and FPy-COF and fabrication of Co-Py-CON and Co-FPy-CON. (b,c) Experimental diffraction pattern (red), profile calculated from Le Bail fitting (black) and residual (blue), and pattern simulated from the structural model (green) for Py-COF (b) and FPy-COF (c); reflection positions are shown by tick marks. The observed peak shift can be accounted for by a small difference in the experimental and simulated unit cells. (d) Nitrogen adsorption isotherms (filled symbols) and desorption isotherms (open symbols) for Py-COF, FPy-COF, Co-Py-CON, and Co-FPy-CON, recorded at 77.3 K.

Examples of COFs include materials that contain bipyridine-based units which have been previously used to stabilize metal atoms within the framework.[14,15] Although these 2D COF materials show strong visible light absorption, utilization of the catalytic metal sites has often been shown to be poor, as expressed by their low turnover numbers (TONs).[30]

Here, we report a new 2D COF, Py-COF, synthesized *via* a Schiff base condensation reaction, that bears metal coordination sites—iminopyridine moieties—that are formed by pyridine units and their adjacent imine groups. A partially fluorinated analogue of Py-COF, FPy-COF, was synthesized with the aim of improving the COF's binding affinity toward CO_2, thus enhancing its ability to enrich CO_2 around the catalytic sites. Exfoliation of bulk 2D COFs yielded covalent organic nanosheets (CONs), which were then loaded with cobalt for photocatalytic CO_2 reduction. We also show that the iminopyridine moiety is a versatile metal coordination site for different transition metals, which has not yet been explored in the context of COF catalysts.

EXPERIMENTAL SECTION

COF Synthesis. All COFs were prepared using a procedure based on the method described here for the synthesis of FPy-COF. A Schlenk tube was charged with 5,5′,5″,5‴-(pyrene-1,3,6,8-tetrayl)-tetrapicolinaldehyde (24.9 mg, 0.04 mmol), 4,4′-diamino-2,2′-difluorobiphenyl (17.6 mg, 0.08 mmol), 1,2-dichlorobenzene (0.5 mL), *n*-butanol (0.5 mL), and aqueous acetic acid (0.1 mL, 6 M). This mixture was homogenized by ultrasonication for 10 min, and the

https://dx.doi.org/10.1021/acs.chemmater.0c01642
Chem. Mater. XXXX, XXX, XXX−XXX

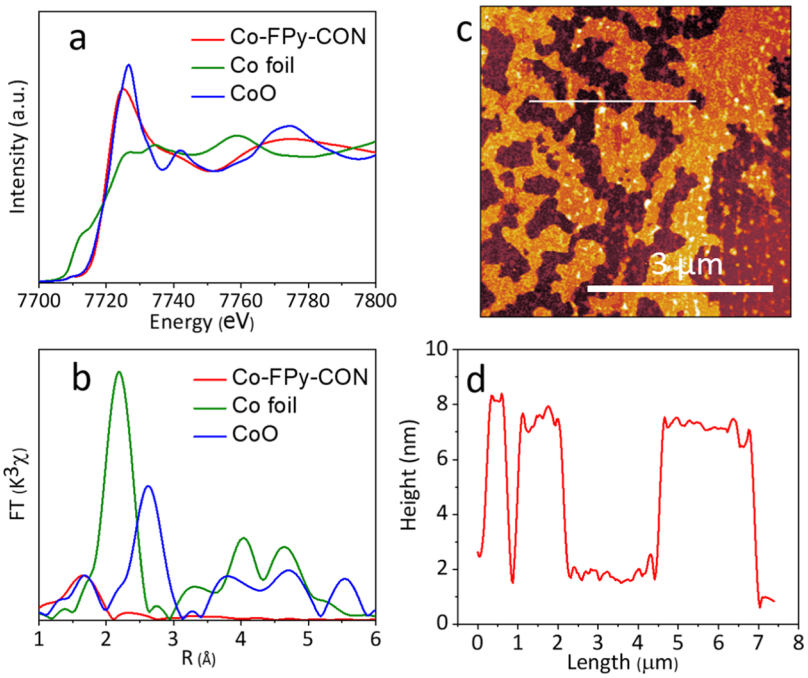

Figure 2. (a,b) X-ray absorption near-edge structure spectra at the Co K-edge (a) and k^3-weighted Fourier-transformed Co K-edge X-ray absorption fine structure spectroscopy (EXAFS) spectra (b) of Co-FPy-CON, CoO, and Co foils. (c) Atomic force microscopy (AFM) image of Co-FPy-CON, with the measured thickness along the line shown in (d).

tube was then flash-frozen at 77 K (liquid N_2 bath) and degassed by three freeze−pump−thaw cycles. The tube was then sealed off and then heated at 120 °C for 7 days. The yellow precipitate was collected by centrifugation (3000 min^{-1}, 3 min) and washed with *N*,*N*-dimethylformamide (100 mL), THF (100 mL), and anhydrous acetone (200 mL). After drying at 120 °C, the product was obtained as a yellow powder (35 mg, 88%). Anal. Calcd for $(C_{68}H_{50}F_4N_8)_n$: C, 77.40; H, 4.78; F, 7.2; N, 10.62. Found: C, 70.68; H, 3.48; N, 9.06.

Cobalt Loading onto CONs. All cobalt loading procedures were based on the method described here for the synthesis of Co-FPy-CON. FPy-COF (20 mg) was mixed with $CoCl_2{\cdot}6H_2O$ (9 mg, 0.0378 mmol) in acetonitrile (20 mL), and the resulting suspension was ultrasonicated for 6 h at room temperature. After this, the solid was filtered off and washed with acetonitrile (200 mL). The resulting solid was dried under a vacuum at 60 °C overnight to yield Co-FPy-CON. The cobalt content of Co-FPy-CON was determined by inductively coupled plasma-optical emission spectrometry to be 2.1 wt %.

Carbon Dioxide Reduction Experiments. A quartz flask was charged with the COF nanosheet powder (1 mg), 2,2′-bipyridyl (1.5 mg), acetonitrile, water, and triethanolamine (TEOA) (3:1:1 vol mixture, 5 mL) and sealed with a septum. The resulting suspension was ultrasonicated for 5 min and then purged with CO_2 for 5 min. The reaction mixture was illuminated with a 300 W Newport Xe light source (model: 6258, Ozone-free) equipped with a $\lambda > 420$ nm cutoff filter. Gaseous products were taken with a gas-tight syringe and run on a Shimadzu GC-2014 gas chromatograph equipped with a ShinCarbon ST micropacked column (Restek 80−100 mesh, 2 m length, and 0.53 mm inner diameter) and a thermal conductivity detector calibrated against standard gas mixtures of known concentration.

RESULTS AND DISCUSSION

Two COFs, Py-COF and FPy-COF, were synthesized *via* Schiff base condensation of 5,5′,5″,5‴-(pyrene-1,3,6,8-tetrayl)-tetrapicolinaldehyde with aromatic diamines (Figure 1a). The COFs were then ultrasonicated in acetonitrile containing $CoCl_2$, resulting in exfoliated, Co-loaded COF nanosheets, Co-Py-CON and Co-FPy-CON (Figure 1a). The Fourier transform infrared (FT-IR) spectra of the materials were similar before and after ultrasonication in the presence of $CoCl_2$ (Figure S2), indicating that the COFs did not undergo decomposition during delamination and metal loading. The experimental powder X-ray diffraction (PXRD) patterns of Py-COF show diffraction peaks at 3.27, 4.77, 6.55, 7.56, and 9.83°, assigned to the (110), (210), (220), (130), and (330) planes, respectively (Figure 1b). The isostructural FPy-COF shows similar levels of crystallinity, and the diffraction peaks at 3.20, 6.50, 7.30, and 9.62° were assigned to the (110), (220), (130), and (330) planes, respectively (Figure 1c). The unit cell parameters extracted by Le Bail refinements are similar to the parameters obtained by structure simulations. The simulated diffraction profiles for the AA stacking model for both Py-COF (Figure 1b) and FPy-COF (Figure 1c) agree well with the experimental PXRD data. Both Co-Py-CON and Co-FPy-CON are less crystalline than their pristine COF counterparts (Figures S7 and S8), as a result of the processes of exfoliation and metal loading.[31]

Nitrogen sorption experiments were performed at 77 K, and the Brunauer−Emmett−Teller (BET) surface areas of Py-COF and FPy-COF were found to be 924 and 1136 $m^2\ g^{-1}$, respectively. These experimental surface areas are lower than those derived from the atomistic models of perfectly crystalline structures (2168 and 2044 $m^2\ g^{-1}$, respectively).[25,28] The pore diameters derived for Py-COF and FPy-COF by fitting the nonlocal density functional theory models to the N_2 isotherms were 24.5 and 23.8 Å, respectively. Both COFs gave rise to nitrogen isotherms, with the shapes consistent with mesoporous and sequential, multilayer pore filling (Figure 1d). Exfoliation and metalation resulted in a reduction of the BET surface area to 207 and 238 $m^2\ g^{-1}$ for Co-Py-CON and Co-FPy-CON, respectively, though both materials were still microporous. Co-FPy-CON shows higher CO_2 adsorption amounts and larger isosteric heats than its nonfluorinated

https://dx.doi.org/10.1021/acs.chemmater.0c01642
Chem. Mater. XXXX, XXX, XXX−XXX

counterpart Co-Py-CON. Likewise, the bulk FPy-COF material shows a better CO_2 adsorption performance than its nonfluorinated counterpart (Figures S9–S12). This can be attributed to the enhanced binding between CO_2 and the fluorinated moieties of the COF, owing to the latter's ability to polarize CO_2.[32,33]

The cobalt species in Co-FPy-CON were studied using X-ray absorption spectroscopy at the Co K-edge, in reference to the standard Co foil and cobalt(II)oxide (CoO). The Co K-edge absorption edge position on Co-FPy-CON is similar to that on CoO, meaning that the Co atoms on Co-FPy-CON are in the oxidation state of +2. These results are consistent with the X-ray photoelectron spectroscopy (XPS) data (Figure S19). The coordination environment of cobalt in Co-FPy-CON was further investigated by extended EXAFS. The Fourier-transformed R-space spectrum of Co foil shows a sharp peak at around 2.2 Å (Figure 2b), corresponding to the Co–Co bond, which is absent in the spectrum of Co-FPy-CON. Similarly, the peak centered at 2.6 Å that corresponds to the shortest Co···Co distance in CoO is also absent for Co-FPy-CON. For Co-FPy-CON, the only distinct peak is centered around 1.6 Å, which can be attributed to the Co–N bonds,[34] in line with the first peak (at 1.6 Å) of the CoO spectrum being assigned to the Co–O bond. By EXAFS curve fitting (Figure S20 and Table S3), the coordination number of the isolated Co atoms in Co-FPy-CON was determined to be 6.0, with a bond length of 2.13 Å. This shows that the Co atom is ligated onto the iminopyridine moiety of Co-FPy-CON, with the solvent acetonitrile molecules also participating in coordination with Co, as shown in the schematic diagram in Figure 1a. Although there are three different types of Co–N bonds in Co-FPy-CON, only one peak in the EXAFS spectrum is assigned to the Co–N pair. This is because of the small differences in the Co–N bond lengths, approximately 0.1 Å,[35,36] which are not distinguishable in the EXAFS spectra. These EXAFS results show that short Co···Co distances are not present in Co-FPy-CON; hence, Co centers can be considered atomically distributed in the material. In the final catalytic system, an additional 2,2′-bipyridine was required to form catalytic Co centers (Figure 1a).[14]

Scanning electron microscopy images (SEM) for both Co-Py-CON and Co-FPy-CON show a microball-like agglomerate morphology (Figure S13). Elemental mapping images of high-angle annular dark-field scanning transmission electron microscopy (HAADF-STEM) for Co-Py-CON (Figure S14) show the uniform distribution of C, N, Cl, and Co in the material. HAADF-STEM of Co-FPy-CON shows that C, N, F, Cl, and Co are distributed uniformly over the sample (Figure S15). Co clusters or nanoparticles were not observed by HAADF-STEM (Figure S17a), indicating that the Co species were too small to be resolved. Aberration-corrected HAADF-STEM was therefore used to characterize Co-FPy-CON. Figure S17b shows that isolated Co atoms are distributed on the COF matrix, identified by the bright dots, with some highlighted by the red cycles. The AFM images of Co-FPy-CON show that the nanosheets were thin stacks of COF layers, with thicknesses ranging from 1.9 to 4.4 nm (Figure 2c,d).

Next, we used density functional theory (DFT) and time-dependent (TD-)DFT calculations—performed on the representative molecular models $[Co\text{-}Py(L)]^{2+}$ and $[Co\text{-}FPy(L)]^{2+}$ of Co-Py-COF and Co-FPy-COF, respectively—to calculate the energy levels of the COFs. We find that the electron affinity (EA) and the ionization potential (IP) of both COFs straddle the reduction potential of CO_2 to CO, as well as the proton reduction potential, and the oxidation potential of TEOA (Figure 3a). This provides a thermodynamic explanation for the ability of both COFs to drive CO_2 reduction to CO in the presence of the sacrificial agent TEOA.

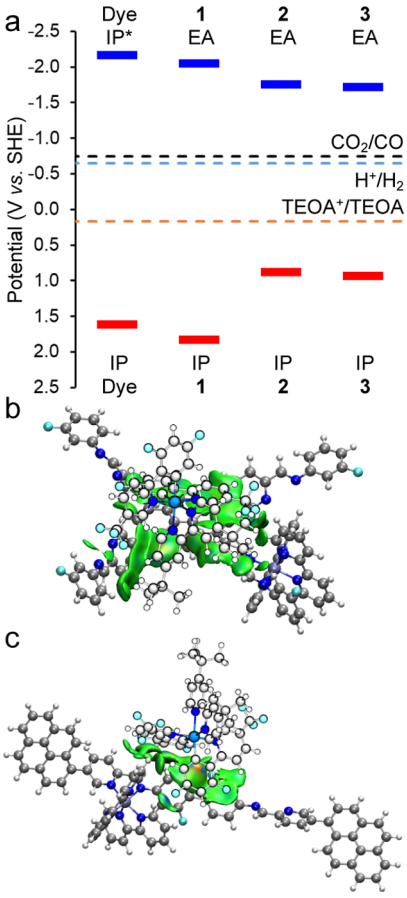

Figure 3. (a) (TD-)DFT-predicted potentials of the free-charge carriers (IP and EA) and excitons (IP*) of the dye, the molecular catalyst $[Co(Bpy)_3]^{2+}$ (1), and the representative fragments $[Co\text{-}Py(L)]^{2+}$ (2) and $[Co\text{-}FPy(L)]^{2+}$ (3) of Co-Py-COF and Co-FPy-COF, respectively. Dashed colored lines indicate the potentials for CO_2 reduction to CO, proton reduction, and TEOA oxidation, respectively. DFT-optimized adsorption configuration of the dye on the pyrene moiety (b) or the difluorobiphenyl moiety (c) of Co-FPy-COF. Colored isosurfaces are the intermolecular interactions identified and quantified by noncovalent interaction analyses. COF fragments are shown in full atomic, ball-and-stick representation, with the dye shown as a lighter sketch.

The photocatalytic CO_2 reduction activity of Co-FPy-CON was then tested in water, acetonitrile, and TEOA (1:3:1 vol mixtures) under visible light irradiation (λ > 420 nm, 300 W Xe light source). Under these conditions, the system showed low activity, and only trace amounts of carbon monoxide were produced (Figure S28).

We suspected that light harvesting and/or the following energy transfer might be responsible for the low activity of Co-FPy-CON. We therefore employed $(Ir[dF(CF_3)\text{-}ppy]_2(dtbpy))PF_6$ as a photosensitizer in conjunction with Co-FPy-CON and found that the system worked efficiently, producing carbon monoxide at a rate of 10.1 μmol over 6 h (TON = 28.1) with a selectivity of 76% over the competing H_2

https://dx.doi.org/10.1021/acs.chemmater.0c01642
Chem. Mater. XXXX, XXX, XXX–XXX

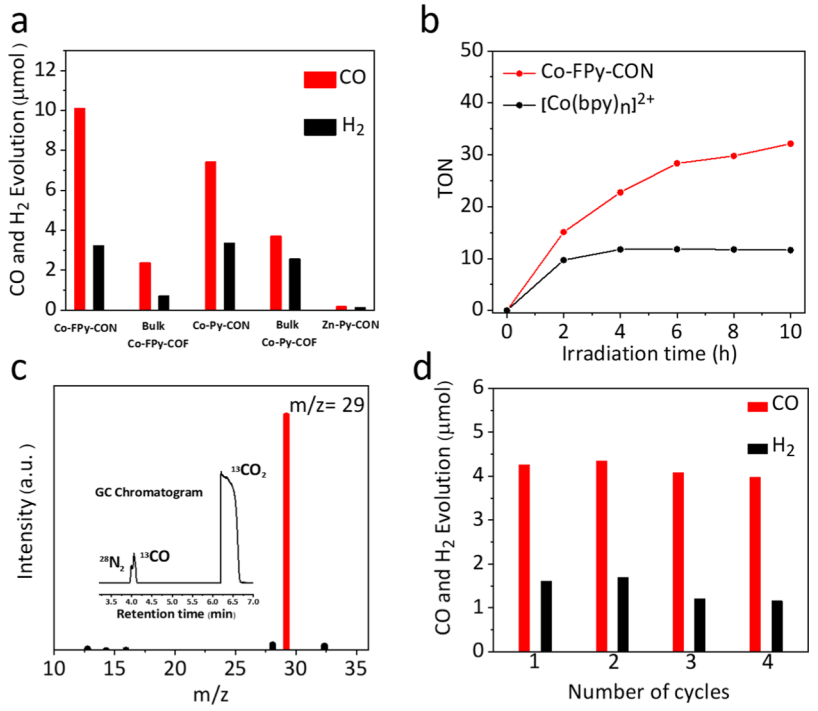

Figure 4. (a) CO and H_2 production by the nanosheet (denoted CON) and bulk (denoted COF) of Co-FPy-COF, Co-Py-COF, and Co-Bp-COF, over 6 h under visible light irradiation (λ > 420 nm, 300 W Xe light source), with $(Ir[dF(CF_3)ppy]_2(dtbpy))PF_6$ as a photosensitizer. (b) TONs of CO production by Co-FPy-CON and $[Co(Bpy)_n]^{2+}$ under visible light irradiation (λ > 420 nm, 300 W Xe light source), with $(Ir[dF(CF_3)ppy]_2(dtbpy))PF_6$ as a photosensitizer. (c) Mass spectrum of ^{13}CO produced using Co-FPy-CON as the catalyst in the photocatalytic reduction of $^{13}CO_2$; inset: the corresponding gas chromatogram. (d) CO and H_2 production by Co-FPy-CON over multiple 2 h repeat runs. The sample was degassed, and 1 μmol of $(Ir[dF(CF_3)ppy]_2(dtbpy))PF_6$ was added after each run.

generation reaction (Figure 4a,b and Table S7). The $(Ir[dF(CF_3)ppy]_2(dtbpy))PF_6$ dye on its own was found to be inactive, producing no measurable CO after 7 h (Table S7).

The predicted relative energy levels of the dye and the molecular COF models confirm that the excited electrons and excitations on the dye are thermodynamically allowed to be transferred to the COFs (Figure 3a), in line with the dye sensitization effects that we observed experimentally. The Monte Carlo simulations of dye adsorption on a single Co-FPy-COF layer, followed by noncovalent interaction analyses using DFT calculations of cluster models (Figure 3b,c), show that the dye binds strongly to both the pyrene moiety and the difluorobiphenyl moiety of Co-FPy-COF. Both binding sites are in the immediate vicinity of the photocatalytic Co site, beneficial to the charge transfer from the dye to the COF.

Analyses based on the DFT results of the excited-state, interfragment charge transfer between the building units of Co-FPy-COF and Co-Py-COF indicate that negligible amounts of electrons are transferred between the pyrene fragment and the Co-loaded iminopyridine fragment (Table S5), for the first three low-energy, excited electronic states with an appreciable oscillator strength. The corresponding intrafragment electron redistributions within the individual fragments show that these low-energy states are local excitations, primarily located on the Co-loading iminopyridine moieties (Table S6). Further analyses of the natural transition orbitals for these electronic transitions indicate a metal-to-iminopyridine excitation mechanism, which is similar to the excitation of the molecular catalyst $[Co(Bpy)_3]^{2+}$ in solution.

The fact that the COF does not act as a photocatalyst on its own, requiring $[(Ir[dF(CF_3)ppy]_2(dtbpy))PF_6]$ as a photosensitizer to facilitate the catalytic reduction of CO_2, together with the computational results, indicates that the function of the COFs appears to be to allow the charge to be transferred and to provide metal coordination sites for the cobalt catalyst.

The isotope labeling study for $^{13}CO_2$ reduction using mass spectrometry confirmed that CO was produced from $^{13}CO_2$ (Figure 4c), ruling out the degradation of the photosensitizer, photocatalyst, or scavenger as the source of the produced CO. No hydrocarbon or alcohol products were observed. An EQE of 6.6% at 420 nm for the CO evolution of Co-FPy-CON was determined. This is higher than the previously reported EQE values of Ni-TpBpy-COF and Co-ZIF-9, both with $[Ru(bpy)_3]Cl_2$ as the photosensitizer and TEOA as the scavenger at 420 nm.[3,14] The bulk sample of Co-FPy-COF produced 2.36 μmol CO over 6 hours (TON = 15.5), 4.3 times lower than that of Co-FPy-CON, which may be partly attributed to the lower loading of Co in Co-FPy-COF (0.9 vs 2.1 wt %, as in the COF and CON, respectively). Co-Py-CON was less active than its fluorinated counterpart, producing 7.4 μmol of CO over 6 h (TON = 10.9). This might be attributed to the fact that Co-FPy-CON has a stronger binding affinity for CO_2 (Figures S11 and 12) and to the dye (Figure S27), despite having a lower Co loading (2.1 wt %) than Co-Py-CON (4.0 wt %). The bulk sample of Co-Py-COF also showed a lower CO production than its CON counterpart.

Bp-COF was synthesized as a comparison, which incorporates pyrene units and bipyridine sites instead of the iminopyridine sites, as in Py-COF and FPy-COF, for ligation of the Co complex (Section S2, Supporting Information). Under the same conditions, Co-Bp-CON showed a photocatalytic performance comparable to Co-Py-CON, though producing less CO with a lower CO/H_2 selectivity. This suggests that it may be a promising, general strategy to

https://dx.doi.org/10.1021/acs.chemmater.0c01642
Chem. Mater. XXXX, XXX, XXX−XXX

incorporate iminopyridine-based moieties into COFs as metal coordination sites for introducing catalytically active metal centers into porous materials. Indeed, it was straightforward to prepare Zn-FPy-CON, which showed a measurable CO_2 reduction activities (Table S7).

Over a total of 10 h of irradiation under visible light (Figure 4b), Co-FPy-CON showed a TON of 32.1, 2.8 times higher than its homogeneous counterpart $[Co(bpy)_n]^{2+}$, which was deactivated after 3 h, consistent with previous studies.[37−39] Repeat experiments showed that the recycled Co-FPy-CON catalyst retained its photocatalytic activity over four 2 h runs (Figure 4d) when fresh $(Ir[dF(CF_3)ppy]_2(dtbpy))PF_6$ was added. It appears therefore that the decrease in activity observed for the extended 10 h run (Figure 4b) is due to dye degradation, and Co-FPy-CON appears to be stable under the photocatalysis conditions. This is further supported by the post-illumination FT-IR spectra (Figure S21) of the sample after the repeat experiments. Furthermore, the XPS measurements of the sample confirmed that the oxidation state of Co remained at +2 after the catalysis experiments (Figure S22). Only trace amounts of cobalt (6.6 ppm) were found in the filtered solution after photocatalysis, measured by inductively coupled plasma-optical emission spectrometry, suggesting that Co-FPy-CON was not demetallized during the catalysis. No iridium was detected, indicating that neither the photodeposition of iridium onto the CONs occurs nor the dye was absorbed onto the surface.

CONCLUSIONS

COF nanosheets loaded with single Co sites for photocatalytic CO_2 reduction have been shown to be efficient in the presence of a dye and a hole scavenger. Co-FPy-CON achieved a high CO production of 10.1 μmol and a CO/H_2 selectivity of 76%, over 6 h irradiation under visible light (TON = 28.1). A high EQE of 6.6% was determined under 420 nm irradiation. The performance of Co-FPy-CON is comparable to the state-of-the-art heterogeneous catalysts in the literature under comparable conditions (Table S8). The COF material in this case does not appear to act as a photocatalyst itself but instead as a semiconductor support that transfers charge carriers that are generated in the dye to the cobalt centers, which are the active sites. Nevertheless, COFs offer advantages, such as being tunable, and can be exfoliated, and we found across the systems studied here that the ultrathin COF nanosheets were shown to consistently outperform their corresponding bulk materials in visible light-driven CO_2 reduction to CO. Finally, the iminopyridine moiety seems to be a promising alternative to bipyridine as metal coordination sites for the ligation of catalytic metal centers into the backbone of porous networks, such as COFs, metal−organic frameworks, and conjugated microporous polymers.

ASSOCIATED CONTENT

Supporting Information

The Supporting Information is available free of charge at https://pubs.acs.org/doi/10.1021/acs.chemmater.0c01642.

Synthetic procedures, FT-IR spectra, NMR, thermal gravimetric analysis, UV−vis spectra, PXRD patterns, CO_2 adsorption, SEM images, STEM images, AFM images, photoluminescence (PL) spectra and time-correlated single-photon counting experiments, PL quenching data, post-photocatalysis characterization data, and computational details (PDF)

AUTHOR INFORMATION

Corresponding Authors

Linjiang Chen − *Department of Chemistry and Materials Innovation Factory and Leverhulme Research Centre for Functional Materials Design, University of Liverpool, Liverpool L7 3NY, U.K.*; Email: lchen@liverpool.ac.uk

Reiner Sebastian Sprick − *Department of Chemistry and Materials Innovation Factory, University of Liverpool, Liverpool L7 3NY, U.K.; Department of Pure and Applied Chemistry, University of Strathclyde, Glasgow G1 1XL, U.K.*; orcid.org/0000-0002-5389-2706; Email: Sebastian.sprick@strath.ac.uk

Andrew I. Cooper − *Department of Chemistry and Materials Innovation Factory and Leverhulme Research Centre for Functional Materials Design, University of Liverpool, Liverpool L7 3NY, U.K.*; orcid.org/0000-0003-0201-1021; Email: aicooper@liverpool.ac.uk

Authors

Xiaoyan Wang − *Department of Chemistry and Materials Innovation Factory, University of Liverpool, Liverpool L7 3NY, U.K.*

Zhiwei Fu − *Department of Chemistry and Materials Innovation Factory, University of Liverpool, Liverpool L7 3NY, U.K.*

Lirong Zheng − *Beijing Synchrotron Radiation Facility, Institute of High Energy Physics, Chinese Academy of Sciences, Beijing 100049, P. R. China*

Chengxi Zhao − *Department of Chemistry and Materials Innovation Factory, University of Liverpool, Liverpool L7 3NY, U.K.; Key Laboratory for Advanced Materials and School of Chemistry and Molecular Engineering, East China University of Science and Technology, Shanghai 200237, P. R. China*

Xue Wang − *Department of Chemistry and Materials Innovation Factory and Leverhulme Research Centre for Functional Materials Design, University of Liverpool, Liverpool L7 3NY, U.K.*

Samantha Y. Chong − *Department of Chemistry and Materials Innovation Factory, University of Liverpool, Liverpool L7 3NY, U.K.*; orcid.org/0000-0002-3095-875X

Fiona McBride − *Open Innovation Hub for Antimicrobial Surfaces, Surface Science Research Centre, Department of Chemistry, University of Liverpool, Liverpool L69 3BX, U.K.*

Rasmita Raval − *Open Innovation Hub for Antimicrobial Surfaces, Surface Science Research Centre, Department of Chemistry, University of Liverpool, Liverpool L69 3BX, U.K.*

Matthew Bilton − *Imaging Centre at Liverpool, University of Liverpool, Liverpool L69 3GL, U.K.*; orcid.org/0000-0002-0475-2942

Lunjie Liu − *Department of Chemistry and Materials Innovation Factory, University of Liverpool, Liverpool L7 3NY, U.K.*

Xiaofeng Wu − *Department of Chemistry and Materials Innovation Factory, University of Liverpool, Liverpool L7 3NY, U.K.*

Complete contact information is available at: https://pubs.acs.org/10.1021/acs.chemmater.0c01642

Author Contributions

The manuscript was written through contributions of all authors.

https://dx.doi.org/10.1021/acs.chemmater.0c01642
Chem. Mater. XXXX, XXX, XXX−XXX

Notes

The authors declare no competing financial interest.

■ ACKNOWLEDGMENTS

The authors acknowledge funding from the Engineering and Physical Sciences Research Council (EPSRC) (EP/N004884/1), and the Leverhulme Trust *via* the Leverhulme Research Centre for Functional Materials Design. X.W., Z.F., C.Z., and L.L. thank the China Scholarship Council for a PhD studentship. The authors thank A. Ciupa for help with GC−MS and Y. Yan and J. Ward for useful discussions.

■ REFERENCES

(1) Inoue, T.; Fujishima, A.; Konishi, S.; Honda, K. Photoelectrocatalytic Reduction of Carbon Dioxide in Aqueous Suspensions of Semiconductor. *Nature* **1979**, *277*, 637−638.

(2) White, J. L.; Baruch, M. F.; Pander, J. E.; Hu, Y.; Fortmeyer, I. C.; Park, J. E.; Zhang, T.; Liao, K.; Gu, J.; Yan, Y.; Shaw, T. W.; Abelev, E.; Bocarsly, A. B. Light-Driven Heterogeneous Reduction of Carbon Dioxide: Photocatalysts and Photoelectrodes. *Chem. Rev.* **2015**, *115*, 12888−12935.

(3) Wang, S.; Yao, W.; Lin, J.; Ding, Z.; Wang, X. Cobalt Imidazolate Metal-Organic Frameworks Photosplit CO_2 under Mild Reaction Conditions. *Angew. Chem., Int. Ed.* **2014**, *53*, 1034−1038.

(4) Rao, H.; Schmidt, L. C.; Bonin, J.; Robert, M. Visible-Light-Driven Methane Formation from CO_2 with a Molecular Iron Catalyst. *Nature* **2017**, *548*, 74−77.

(5) Takeda, H.; Ohashi, K.; Sekine, A.; Ishitani, O. Photocatalytic CO_2 Reduction Using Cu(I) Photosensitizers with a Fe(II) Catalyst. *J. Am. Chem. Soc.* **2016**, *138*, 4354−4357.

(6) Wang, Y.; Liu, X.; Han, X.; Godin, R.; Chen, J.; Zhou, W.; Jiang, C.; Thompson, J.; Mustafa, K.; Shevlin, S.; Durrant, J.; Guo, Z.; Tang, J. Unique hole-accepting carbon-dots promoting selective carbon dioxide reduction nearly 100% to methanol by pure water. *Nat. Commun.* **2020**, *11*, 2531.

(7) Kuehnel, M. F.; Sahm, C. D.; Neri, G.; Lee, J. R.; Orchard, K. L.; Cowan, A. J.; Reisner, E. ZnSe Quantum Dots Modified with a Ni(Cyclam) Catalyst for Efficient Visible-Light Driven CO_2 Reduction in Water. *Chem. Sci.* **2018**, *9*, 2501−2509.

(8) Roy, S.; Reisner, E. Visible-Light-Driven CO_2 Reduction by Mesoporous Carbon Nitride Modified with Polymeric Cobalt Phthalocyanine. *Angew. Chem., Int. Ed.* **2019**, *58*, 12180−12184.

(9) McMorn, P.; Hutchings, G. J. Heterogeneous Enantioselective Catalysts: Strategies for the Immobilisation of Homogeneous Catalysts. *Chem. Soc. Rev.* **2004**, *33*, 108−122.

(10) Wang, W.; Wang, S.; Ma, X.; Gong, J. Recent Advances in Catalytic Hydrogenation of Carbon Dioxide. *Chem. Soc. Rev.* **2011**, *40*, 3703−3727.

(11) Deng, X.; Qin, Y.; Hao, M.; Li, Z. MOF-253-Supported Ru Complex for Photocatalytic CO_2 Reduction by Coupling with Semidehydrogenation of 1,2,3,4-Tetrahydroisoquinoline (THIQ). *Inorg. Chem.* **2019**, *58*, 16574−16580.

(12) Deng, X.; Albero, J.; Xu, L.; García, H.; Li, Z. Construction of a Stable Ru−Re Hybrid System Based on Multifunctional MOF-253 for Efficient Photocatalytic CO_2 Reduction. *Inorg. Chem.* **2018**, *57*, 8276−8286.

(13) Sun, D.; Gao, Y.; Fu, J.; Zeng, X.; Chen, Z.; Li, Z. Construction of a Supported Ru Complex on Bifunctional MOF-253 for Photocatalytic CO_2 Reduction under Visible Light. *Chem. Commun.* **2015**, *51*, 2645−2648.

(14) Zhong, W.; Sa, R.; Li, L.; He, Y.; Li, L.; Bi, J.; Zhuang, Z.; Yu, Y.; Zou, Z. A Covalent Organic Framework Bearing Single Ni Sites as a Synergistic Photocatalyst for Selective Photoreduction of CO_2 to CO. *J. Am. Chem. Soc.* **2019**, *141*, 7615−7621.

(15) Yang, S.; Hu, W.; Zhang, X.; He, P.; Pattengale, B.; Liu, C.; Cendejas, M.; Hermans, I.; Zhang, X.; Zhang, J.; Huang, J. 2D Covalent Organic Frameworks as Intrinsic Photocatalysts for Visible Light-Driven CO_2 Reduction. *J. Am. Chem. Soc.* **2018**, *140*, 14614−14618.

(16) Lu, M.; Liu, J.; Li, Q.; Zhang, M.; Liu, M.; Wang, J. L.; Yuan, D. Q.; Lan, Y. Q. Rational Design of Crystalline Covalent Organic Frameworks for Efficient CO_2 Photoreduction with H_2O. *Angew. Chem., Int. Ed.* **2019**, *58*, 12392−12397.

(17) Banerjee, T.; Haase, F.; Savasci, G.; Gottschling, K.; Ochsenfeld, C.; Lotsch, B. V. Single Site Photocatalytic H_2 Evolution from Covalent Organic Frameworks with Molecular Cobaloxime Co-Catalysts. *J. Am. Chem. Soc.* **2017**, *139*, 16228−16234.

(18) Biswal, B. P.; Vignolo-González, H. A.; Banerjee, T.; Grunenberg, L.; Savasci, G.; Gottschling, K.; Nuss, J.; Ochsenfeld, C.; Lotsch, B. V. Sustained Solar H_2 Evolution from a Thiazolo[5,4-d]Thiazole-Bridged Covalent Organic Framework and Nickel-Thiolate Cluster in Water. *J. Am. Chem. Soc.* **2019**, *141*, 11082−11092.

(19) Zhang, H.; Wei, J.; Dong, J.; Liu, G.; Shi, L.; An, P.; Zhao, G.; Kong, J.; Wang, X.; Meng, X.; Zhang, J.; Ye, J. Efficient Visible-Light-Driven Carbon Dioxide Reduction by a Single-Atom Implanted Metal−Organic Framework. *Angew. Chem., Int. Ed.* **2016**, *55*, 14310−14314.

(20) Jiao, L.; Jiang, H.-L. Metal-Organic-Framework-Based Single-Atom Catalysts for Energy Applications. *Chem* **2019**, *5*, 786−804.

(21) Fu, Y.; Sun, D.; Chen, Y.; Huang, R.; Ding, Z.; Fu, X.; Li, Z. An Amine-Functionalized Titanium Metal−Organic Framework Photocatalyst with Visible-Light-Induced Activity for CO_2 Reduction. *Angew. Chem., Int. Ed.* **2012**, *51*, 3364−3367.

(22) Sun, D.; Fu, Y.; Liu, W.; Ye, L.; Wang, D.; Yang, L.; Fu, X.; Li, Z. Studies on Photocatalytic CO_2 Reduction over NH_2-Uio-66(Zr) and Its Derivatives: Towards a Better Understanding of Photocatalysis on Metal−Organic Frameworks. *Chem.—Eur. J.* **2013**, *19*, 14279−14285.

(23) Wang, D.; Huang, R.; Liu, W.; Sun, D.; Li, Z. Fe-Based MOFs for Photocatalytic CO_2 Reduction: Role of Coordination Unsaturated Sites and Dual Excitation Pathways. *ACS Catal.* **2014**, *4*, 4254−4260.

(24) Chen, Y.; Wang, D.; Deng, X.; Li, Z. Metal−organic frameworks (MOFs) for photocatalytic CO_2 reduction. *Catal. Sci. Technol.* **2017**, *7*, 4893−4904.

(25) Wang, X.; Chen, L.; Chong, S. Y.; Little, M. A.; Wu, Y.; Zhu, W.-H.; Clowes, R.; Yan, Y.; Zwijnenburg, M. A.; Sprick, R. S.; Cooper, A. I. Sulfone-Containing Covalent Organic Frameworks for Photocatalytic Hydrogen Evolution from Water. *Nat. Chem.* **2018**, *10*, 1180−1189.

(26) Banerjee, T.; Gottschling, K.; Savasci, G.; Ochsenfeld, C.; Lotsch, B. V. H2 Evolution with Covalent Organic Framework Photocatalysts. *ACS Energy Lett.* **2018**, *3*, 400−409.

(27) Pachfule, P.; Acharjya, A.; Roeser, J.; Langenhahn, T.; Schwarze, M.; Schomaecker, R.; Thomas, A.; Schmidt, J. Diacetylene Functionalized Covalent Organic Framework (COF) for Photocatalytic Hydrogen Generation. *J. Am. Chem. Soc.* **2017**, *140*, 1423−1427.

(28) Fu, Z.; Wang, X.; Gardner, A. M.; Wang, X.; Chong, S. Y.; Neri, G.; Cowan, A. J.; Liu, L.; Li, X.; Vogel, A.; Clowes, R.; Bilton, M.; Chen, L.; Sprick, R. S.; Cooper, A. I. A Stable Covalent Organic Framework for Photocatalytic Carbon Dioxide Reduction. *Chem. Sci.* **2020**, *11*, 543−550.

(29) Wang, S.; Hai, X.; Ding, X.; Jin, S.; Xiang, Y.; Wang, P.; Jiang, B.; Ichihara, F.; Oshikiri, M.; Meng, X.; Li, Y.; Matsuda, W.; Ma, J.; Seki, S.; Wang, X.; Huang, H.; Wada, Y.; Chen, H.; Ye, J. Intermolecular cascaded π-conjugation channels for Electron Delivery Powering CO_2 Photoreduction. *Nat. Commun.* **2020**, *11*, 1149.

(30) Lu, M.; Li, Q.; Liu, J.; Zhang, F.-M.; Zhang, L.; Wang, J.-L.; Kang, Z.-H.; Lan, Y.-Q. Installing Earth-Abundant Metal Active Centers to Covalent Organic Frameworks for Efficient Heterogeneous Photocatalytic CO_2 Reduction. *Appl. Catal., B* **2019**, *254*, 624−633.

(31) Bunck, D. N.; Dichtel, W. R. Bulk Synthesis of Exfoliated Two-Dimensional Polymers Using Hydrazone-Linked Covalent Organic Frameworks. *J. Am. Chem. Soc.* **2013**, *135*, 14952−14955.

https://dx.doi.org/10.1021/acs.chemmater.0c01642
Chem. Mater. XXXX, XXX, XXX−XXX

(32) Alahmed, A. H.; Briggs, M. E.; Cooper, A. I.; Adams, D. J. Post-Synthetic Fluorination of Scholl-Coupled Microporous Polymers for Increased CO_2 Uptake and Selectivity. *J. Mater. Chem. A* **2019**, *7*, 549−557.
(33) Li, G.; Zhang, B.; Wang, Z. Facile Synthesis of Fluorinated Microporous Polyaminals for Adsorption of Carbon Dioxide and Selectivities over Nitrogen and Methane. *Macromolecules* **2016**, *49*, 2575−2581.
(34) Chen, C.; Wu, T.; Wu, H.; Liu, H.; Qian, Q.; Liu, Z.; Yang, G.; Han, B. Highly Effective Photoreduction of CO_2 to CO Promoted by Integration of CdS with Molecular Redox Catalysts through Metal-Organic Frameworks. *Chem. Sci.* **2018**, *9*, 8890−8894.
(35) Hojilla Atienza, C. C.; Bowman, A. C.; Lobkovsky, E.; Chirik, P. J. Photolysis and Thermolysis of Bis(Imino)Pyridine Cobalt Azides: C-H Activation from Putative Cobalt Nitrido Complexes. *J. Am. Chem. Soc.* **2010**, *132*, 16343−16345.
(36) Bowman, A. C.; Milsmann, C.; Hojilla Atienza, C. C.; Lobkovsky, E.; Wieghardt, K.; Chirik, P. J. Synthesis and Molecular and Electronic Structures of Reduced Bis(Imino)Pyridine Cobalt Dinitrogen Complexes: Ligand versus Metal Reduction. *J. Am. Chem. Soc.* **2010**, *132*, 1676−1684.
(37) Liu, C.; Dubois, K. D.; Louis, M. E.; Vorushilov, A. S.; Li, G. Photocatalytic CO_2 Reduction and Surface Immobilization of a Tricarbonyl Re(I) Compound Modified with Amide Groups. *ACS Catal.* **2013**, *3*, 655−662.
(38) Guo, Z.; Cheng, S.; Cometto, C.; Anxolabéhère-Mallart, E.; Ng, S.-M.; Ko, C.-C.; Liu, G.; Chen, L.; Robert, M.; Lau, T.-C. Highly Efficient and Selective Photocatalytic CO_2 Reduction by Iron and Cobalt Quaterpyridine Complexes. *J. Am. Chem. Soc.* **2016**, *138*, 9413−9416.
(39) Won, D.-I.; Lee, J.-S.; Ji, J.-M.; Jung, W.-J.; Son, H.-J.; Pac, C.; Kang, S. O. Highly Robust Hybrid Photocatalyst for Carbon Dioxide Reduction: Tuning and Optimization of Catalytic Activities of Dye/TiO_2/Re(I) Organic-Inorganic Ternary Systems. *J. Am. Chem. Soc.* **2015**, *137*, 13679−13690.

https://dx.doi.org/10.1021/acs.chemmater.0c01642
Chem. Mater. XXXX, XXX, XXX−XXX